

International Journal of Modern Physics D  
© World Scientific Publishing Company

## A Parameterized Variable Dark Energy Model: Structure Formation and Observational Constraints

S Arbabi Bidgoli

*Institute for Studies in Theoretical Physics and Mathematics, P.O.Box 19395-5531, Tehran, Iran*  
*arbabi@ipm.ir*

M S Movahed

*Institute for Studies in Theoretical Physics and Mathematics, P.O.Box 19395-5531, Tehran, Iran*  
*Department of Physics, Sharif University of Technology, P.O.Box 11365-9161, Tehran, Iran*  
*m.s.movahed@mehr.sharif.edu*

S Rahvar

*Institute for Studies in Theoretical Physics and Mathematics, P.O.Box 19395-5531, Tehran, Iran*  
*Department of Physics, Sharif University of Technology, P.O.Box 11365-9161, Tehran, Iran*  
*rahvar@sharif.edu*

Received Day Month Year

Revised Day Month Year

Communicated by Managing Editor

In this paper we investigate a simple parameterization scheme of the quintessence model given by Wetterich (2004). The crucial parameter of this model is the bending parameter  $b$ , which is related to the amount of dark energy in the early universe. Using the linear perturbation and the spherical infall approximations, we investigate the evolution of matter density perturbations in the variable dark energy model, and obtain an analytical expression for the growth index  $f$ . We show that increasing  $b$  leads to less growth of the density contrast  $\delta$ , and also decreases the growth index. Giving a fitting formula for the growth index at the present time we verify that the approximation relation  $f \simeq \Omega_m^\alpha$  also holds in this model. To compare predictions of the model with observations, we use the Supernovae type Ia (SNIa) Gold Sample and the parameters of the large scale structure determined by the 2-degree Field Galaxy Redshift Survey (2dFGRS). The best fit values for the model parameters by marginalizing on the remained ones, are  $\Omega_m = 0.21^{+0.07}_{-0.06}$ ,  $w_0 = -2.05^{+0.65}_{-2.05}$  and  $b = 4.05^{+7.05}_{-2.25}$  at  $1\sigma$  confidence level. As a final test we calculate the age of universe for different choices of the free parameters in this model and compare it with the age of old stars and some high redshift objects. Then we show that the predictions of this variable dark energy model are consistent with the age observation of old star and can solve the "age crisis" problem.

**Keywords:** theory dark energy; structure formation; observational constraints.

## 1. Introduction

Recent observations of type Ia Supernovae (SNIa) at low and medium redshifts and the cosmic microwave background (CMB) anisotropies strongly indicate that the total matter-energy density of the universe is now dominated by dark energy<sup>1,2,3,4</sup>. The origin and nature of this dark energy term remains unknown. The most obvious theoretical candidate of dark energy is the cosmological constant  $\Lambda$  which has the equation of state  $w = -1$ <sup>5,6,7</sup>. Since the cosmological constant is a physical link between micro and macro scales, two main questions arise. First, the fine-tuning problem asks why the dark energy density today is so small compared to typical particle scales. The dark energy density is of order  $10^{-47}$  GeV<sup>4</sup>, which appears to require the introduction of new mass scale 14 or so orders of magnitude smaller than the electro-weak scale. The second difficulty, the cosmic coincidence problem, states, Since the energy densities of dark energy and dark matter scale so differently during the expansion of universe why are they nearly equal today? To get this coincidence, it appears that their ratio must be set to a specific, infinitesimal value in the very early universe. As an attempt to solve these problems, one can consider a scalar field with a potential and kinetic term which has an equation of state to behave as vacuum energy. The energy density of this field, called quintessence in the cosmological attractor solution follows the energy density of matter and radiation, but remains negligible until recent epoch<sup>8</sup>. In these models the standard cosmological constant  $\Lambda$ -term is replaced by a dynamical, time-dependent component. Many different variable dark energy models have been proposed in the literature, e.g., Wetterich (1988), Ratra & Peebles (1988)<sup>9,10</sup>. For a more complete list of references and a review of this topic see<sup>11</sup>. This is still not a satisfactory physical explanation for the observed values of the cosmological constant term. The quintessence models do not offer a fundamental explanation, instead they are a phenomenological approach to express our inability of understanding the nature of the cosmological constant in terms of a variable scalar field.

Here we examine a generic parameterization of quintessence models given by Wetterich (2004)<sup>12</sup>. In the recent paper<sup>13</sup> some observational constraints have been investigated for this model and the value of present equation of state was assumed  $w_0 \geq -1$  but in this paper we let this parameter to be  $w_0 \leq 0$  and give the best fitting values for  $w_0$ , present matter density and bending parameter. Also in<sup>14</sup> the constraints related to the background evolution have been used. Our motivation for the present work is to see the possible observational effects<sup>15,16,17</sup> of a variable dark energy on the growth of the large scale structure of the universe. To put the rigorous constraints on the parameters of variable dark energy model we use the luminosity distance of Supernovae type Ia (SNIa) of the Gold Sample<sup>4</sup> and large scale structure parameters determined by the 2dFGRS team. The equation of state used for this quintessence model is:

$$w(z; b, w_0) = \frac{w_0}{[1 + b \ln(1 + z)]^2}, \quad (1)$$

where  $w_0$  is the state parameter at the present time and  $b$  is the bending parameter, which expresses the change in the equation of state of dark energy with redshift and is related to the amount of dark energy in the early universe. According to the theory of structure formation, the evolution of structure in the linear and non-linear regimes depends strongly on the background dynamics of universe. Dark energy as a crucial element of cosmic fluid affects the dynamics of the universe and consequently changes the growing rate of structure. By increasing the parameter  $b$  in the model, the universe enters earlier in the phase of dark energy domination and the faster dilution of matter suppresses the formation of further structure. We assume that variable dark energy behaves as a smooth component, so that in our analysis the structure formation is only due to matter condensation, while the variable dark energy alters only the background cosmic dynamical evolution. We mostly work with  $\Omega_{tot} = 1$  which is based on the results of CMB experiments<sup>18</sup>.

This paper is organized as follows. In section 2 we discuss the linear perturbation theory of cosmological structure formation applied to the case of a variable dark energy. Considering the parameters of the model, we compute the evolution of the matter density contrast and the evolution of the growth index. We apply the spherical approximation with different initial conditions for overdense and underdense regions and compare these results with the linear approximation in Section 3. In section 4, we constrain the parameters of model by using high redshift Supernovae type Ia (SNIa) of the Gold sample and the parameters of Large Scale Structure (LSS) determined by 2-degree Field Galaxy Redshift Survey (2dFGRS). As a consistency test we look at the predicted age of universe in the model by comparing with the age of high redshift objects. The conclusions are given in Section 5.

## 2. Linear Newtonian structure formation with variable dark energy

The dynamics of the universe is driven by the Friedmann's equations as:

$$\left(\frac{\dot{a}}{a}\right)^2 + \frac{k}{a^2} = \frac{8\pi G}{3}(\rho_m + \rho_\lambda), \quad (2)$$

$$\dot{\rho}_m + 3\frac{\dot{a}}{a}\rho_m = 0, \quad (3)$$

$$\dot{\rho}_\lambda + 3\frac{\dot{a}}{a}\rho_\lambda[1 + w(a; b, w_0)] = 0, \quad (4)$$

where the dot denotes the derivative with respect to time,  $\rho_m$  and  $\rho_\lambda$  stand for the pressureless matter and quintessence component, respectively. Also  $w(a; b, w_0)$  is given by Eq. (1). As usual,  $k = 0, 1, -1$  indicates a flat, closed and open spacial section. Dynamic equations for each fluid (equations (3) and (4)) are:

$$\rho_m = \rho_m^0 a^{-3}, \quad \rho_\lambda = \rho_\lambda^0 a^{-3(1+\bar{w}(a; b, w_0))}, \quad (5)$$

where  $\bar{w}(z; b, w_0) = w_0/[1 + b \ln(1 + z)]$ . Fig. 1 shows the behavior of  $\bar{w}(z; b, w_0)$  as a function of redshift. We notice that most variation in  $\bar{w}$  takes place at low redshifts

4 *S Arbabi Bidgoli, M S Movahed and S Rahvar*

and that larger values of  $b$  correspond to a more dust-like behavior of dark energy at high redshifts. The redshift of equality of matter and dark energy strongly depends on the choice of parameter  $b$ , as shown in Fig. 2, a universe with a large  $b$  enters the dark energy dominated regime earlier.

The Hubble parameter for a universe composed of dark matter and dark energy is given by:

$$H^2(z; b, w_0) = H_0^2 [\Omega_m (1+z)^3 + \Omega_\Lambda(z; b, w_0) - (\Omega_{tot} - 1)(1+z)^2], \quad (6)$$

with the definitions:

$$\Omega_m = \frac{8\pi G}{3} \frac{\rho_m^0}{H_0^2}, \quad (7)$$

$$\Omega_\Lambda(z; b, w_0) = \frac{8\pi G}{3} \frac{\rho_\Lambda^0}{H_0^2} (1+z)^{3[1+\bar{w}(z; b, w_0)]}, \quad (8)$$

$$\Omega_{tot} = 1 - \frac{k}{H_0^2} = \Omega_m + \Omega_\Lambda, \quad (9)$$

where  $\Omega_\Lambda$  and  $\Omega_m$  are the ratio of the dark energy density and dark matter density to the critical energy density at the present time, respectively.

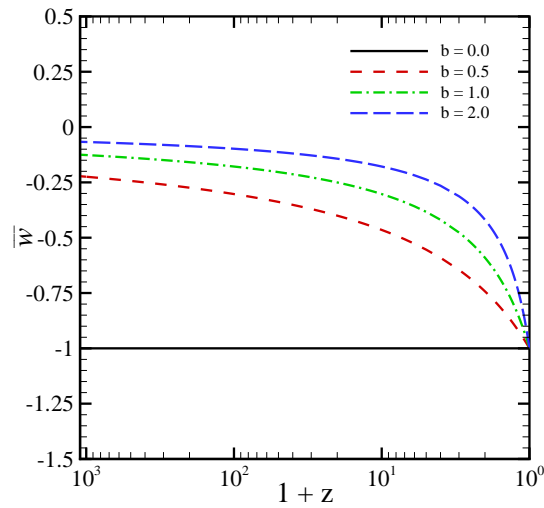


Fig. 1.  $\bar{w}(z; b, w_0)$  in terms of redshift for various bending parameters. Here we choose  $w_0 = -1$ . The slope of the graphs are more sensitive to the bending parameter at low redshifts rather than high redshifts.

Using the continuity and Poisson equations in the expanding FRW universe, the evolution of density contrast,  $\delta = \delta\rho/\bar{\rho}$  in the linear approximation is given by <sup>19,20</sup>:

$$\ddot{\delta} + 2\frac{\dot{a}}{a}\dot{\delta} - (v_s^2 \nabla^2 + 4\pi G\rho_m)\delta = 0. \quad (10)$$

In Eq. (10) the dark energy enters through its influence on the expansion rate  $H(a; b, w_0)$ . The validity of this linear Newtonian approach is restricted to perturbations on the subhorizon scales but large enough where structure formation is still in its linear phase <sup>19,20</sup>. We also assume that the sound horizon of dark energy is much larger than the wavelength of the perturbations, so we do not need to consider the clustering of dark energy. If the perturbation is larger than the Jeans length,  $\lambda_J = \pi^{1/2}v_s/\sqrt{G\rho_m}$ , then Eq. (10) for cold dark matter (CDM) density contrast reduces to:

$$\ddot{\delta} + 2\frac{\dot{a}}{a}\dot{\delta} - 4\pi G\rho_m\delta = 0, \quad (11)$$

The equation that describes the evolution of density contrast with respect to the scale factor is:

$$\frac{d^2\delta}{da^2} + \frac{d\delta}{da} \left[ \frac{\ddot{a}}{\dot{a}^2} + \frac{2H(a; b, w_0)}{\dot{a}} \right] - \frac{3H_0^2}{2\dot{a}^2 a^3} \Omega_m \delta = 0. \quad (12)$$

The numerical solution of Eq. (12) in a Friedmann universe with variable dark energy evolving as given in Eq. (6), is shown in Fig. 3. In the matter dominated era, the density contrast  $\delta$  grows linearly with the scale factor, while we have a deviation from a linear behavior, when dark energy begins to dominate. For larger

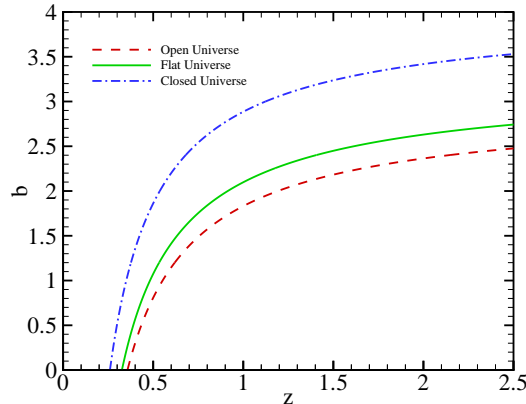


Fig. 2. Redshift of equality of dark energy and dark matter density as a function of the bending parameter  $b$ , for a flat universe (Solid line) with the  $\Omega_m = 0.3$  and  $\Omega_\lambda = 0.7$ , an open universe (dashed line) with  $\Omega_m = 0.2$  and  $\Omega_\lambda = 0.5$  and a closed universe (dot-dashed line) with  $\Omega_m = 1.0$  and  $\Omega_\lambda = 2.0$ . Increasing the bending parameter results in a higher redshift of equality. The present state parameter is set to  $w_0 = -1.0$ .

$b$  (see Fig. 2) the domination of dark energy occurs earlier and the friction term in Eq. (11) increase so the growth of density contrast decreases. The relative difference between the present value of the  $\Lambda$ CDM and the dark energy models is about 2.5% for  $b = 0.1$  and 100% for  $b = 1$ .

In the linear perturbation theory the peculiar velocity field  $\mathbf{v}$  is determined by the density contrast<sup>19,21</sup> :

$$\mathbf{v}(\mathbf{x}) = H_0 \frac{f}{4\pi} \int \delta(\mathbf{y}) \frac{\mathbf{x} - \mathbf{y}}{|\mathbf{x} - \mathbf{y}|^3} d^3\mathbf{y}, \quad (13)$$

where the growth index  $f$  is defined as:

$$f = \frac{d \ln \delta}{d \ln a}. \quad (14)$$

We use the density contrast  $\delta$  to compute the growth index of structure  $f$ , which is an important quantity for the interpretation of peculiar velocities of galaxies, as discussed in<sup>21</sup> for the Newtonian and<sup>22</sup> for the relativistic regime of structure formation. For understanding the physical meaning of the growth index it is helpful to divide the second term of Eq. (11) (friction) by the third (Poisson), which shows that:  $f \propto 2H\dot{\delta}/4\pi G\rho_m\delta$ .

According to equations (12) and (14), the evolution of the growth index is given by:

$$\begin{aligned} \frac{df}{d \ln a} = & -f \left[ 2 - \frac{H_0^2}{2} \left[ \frac{2}{H_0^2} + \frac{\Omega_m}{a^3} + \Omega_\Lambda(a; b, w_0)(1 + 3w(a; b, w_0)) \right] \right] \\ & - f^2 + \frac{3H_0^2}{2a^3} \Omega_m. \end{aligned} \quad (15)$$

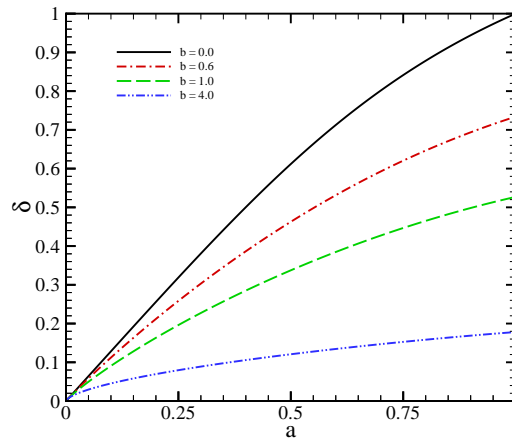


Fig. 3. Evolution of density contrast as a function of scale factor for different bending parameters in the flat universe with  $\Omega_m = 0.3$ ,  $\Omega_\Lambda = 0.7$  and  $w_0 = -1.0$ .

In Fig. 4 we plot the numerical solution of Eq. (15) for the growth index as a function of redshift for  $b = 0$ ,  $b = 1.0$  and  $b = 4.0$ , for various amounts of dark matter and dark energy at the present epoch. The growth index  $f$  has been calculated for models with a cosmological constant earlier and the case of  $b = 0$  corresponds to the  $\Lambda$ CDM model with non-variable cosmological constant, where our results are identical with the earlier results given by <sup>23</sup>. There a fitting formula was given for the dependence of  $f$  on  $\Omega_m$  for the case of a flat universe. The dependence on the cosmological constant was found to be very weak. Here we extend this analysis to models with a variable dark energy, including the bending parameter  $b$  and  $w_0$ . In agreement with the tendency found earlier, we also find that in our case the dependence on  $b$  is not significant at the present time. This fitting formula is as follows:

$$f(\Omega_m, \Omega_\lambda, b, w_0, z = 0) \approx \Omega_m^{0.57} + [-0.030 + 0.019 \exp(-b) - 0.038 w_0] \\ \times \Omega_\lambda^{[1.047 - 0.145 b^{0.51} + (-0.104 - 0.30 b^{1.2}) w_0^3]} - \frac{b^{0.45}}{100}. \quad (16)$$

At the present time the growth index shows mostly a dependence on the matter density of the universe  $\Omega_m$ . But the time evolution of the growth index depends strongly on the choice of the parameters  $\Omega_\lambda$  and  $b$ . Fig. 5 shows the time evolution of the growth index  $f$  for different pairs of  $(\Omega_m, \Omega_\lambda)$ , where the sensitivity to the bending parameter is examined. The main effect is that increasing the bending parameter decreases the growth index for all cases of open, closed and flat universe and results in a lower abundance of structure at the present time. In Fig. 6 the result from numerical solution of Eq. (15) and from fitting formula, Eq. (16), are illustrated. This shows that the growth index is approximated by  $f \sim \Omega_m^\alpha$ .

In the case of a closed universe, the growth index rises to a maximum and descends afterward. This temporal increasing of the growth index is due to the dynamical effect of dark energy that changes the sign of the acceleration from negative to positive and the slope of deceleration parameter  $q = -\ddot{a}/aH^2$ . During the transition phase of the acceleration, the universe reaches its lowest expansion rate and the structures have an opportunity to grow almost exponentially. Increasing the bending parameter suppresses the bump of the growth index (see Fig. 5), because the dominance of the dark energy occurs at earlier times and increases the friction term proportional to the expansion rate.

### 3. Variable Dark energy and nonlinear structure formation in the spherical approximation

A simple approximation for calculating the formation of cosmological objects is the spherical infall model <sup>23,24,25</sup>. In this model we consider an overdense (or an underdense) spherical region, i.e. a positive density perturbation  $\delta > 0$  (or  $\delta < 0$ ) with spherical symmetry. For large enough positive perturbations, this region becomes gravitationally unstable and grows to a bound structure seen in the universe today. In such overdense regions the gravity of the perturbations is able to stop the expansion, turn it around and finally make the particles collapse. This highly nonlinear

8 *S Arbabi Bidgoli, M S Movahed and S Rahvar*

process is usually modeled with a number of simplifying assumptions<sup>19</sup>. Here we also apply this approximation to the case of a negative density perturbation  $\delta < 0$  and take into account a non-constant dark energy term. For  $\delta < 0$  only the initial conditions are different and the dynamical growth of the spherical underdense region is governed by the same equation. Since in the underdense regions the probability of forming galaxies, in particular luminous galaxies is lower,<sup>24</sup>, these regions correspond to voids in the observed galaxy distribution.

We begin with the Friedmann equation with a quintessence term as given in Eq. (6). Until an initial time  $t_i$  we assume the spherical region  $R_i$  to grow with the same

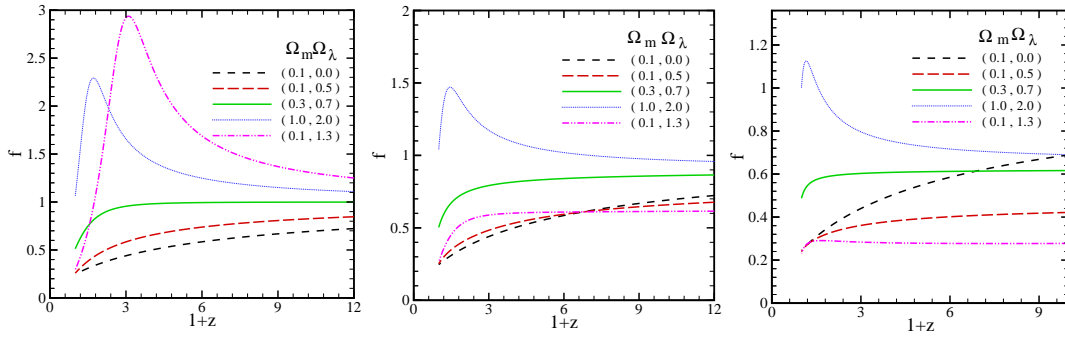


Fig. 4. Growth index versus redshift for pairs of cosmological density parameters  $\Omega_m$  and  $\Omega_\lambda$ . The panels refer to different values of the bending parameter  $b$  and  $w_0 = -1.0$ . Left panel:  $b = 0.0$  corresponds to the case of  $\Lambda$ CDM model. Middle:  $b = 1.0$ . Right:  $b = 4.0$  as an extreme case of the variable dark energy model.

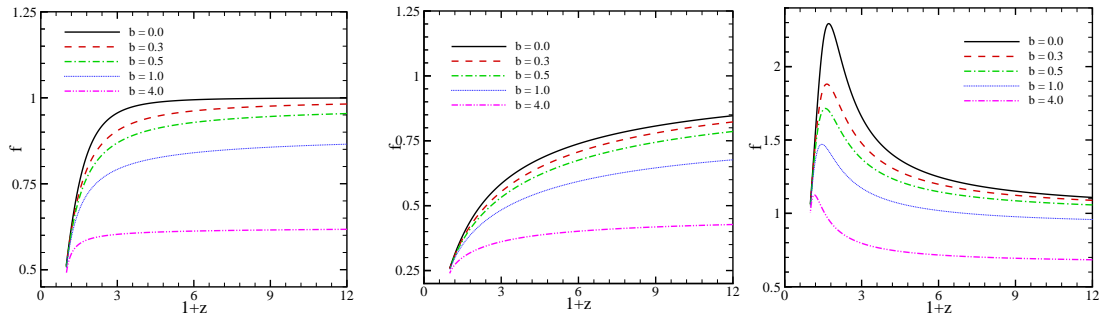


Fig. 5. The effect of bending parameter  $b$  on the evolution of the growth index as a function of redshift in case of different pairs of  $\Omega_m$  and  $\Omega_\lambda$ . Left panel: A flat universe with  $\Omega_m = 0.3$  and  $\Omega_\lambda = 0.7$ . Middle: An open universe with  $\Omega_m = 0.1$  and  $\Omega_\lambda = 0.5$ . Right panel: A closed universe with  $\Omega_m = 1.0$  and  $\Omega_\lambda = 2.0$ .



rate as the background universe:

$$\left(\frac{\dot{R}_i}{R_i}\right)^2 = H_0^2 \left[ \Omega_m a_i^{-3} + \Omega_\lambda a_i^{-3[1+\bar{w}(a_i; b, w_0)]} - (\Omega_{tot} - 1) a_i^{-2} \right], \quad (17)$$

where  $a_i$  is the initial scale factor of the background. At the time  $t_i$  we introduce an initial density perturbation  $\delta_i$  in the matter density  $\Omega_m^i = (1 + \delta_i)\Omega_m a_i^{-3}$ . As long as there is no shell crossing, the matter content inside a shell is constant. As in Section 2, we assume the effect of dark energy to be on much larger scales than the forming structure. This means that the dynamics of the universe is changed by dark energy but at the scale of structures, such as galaxies and clusters of galaxies the pressure of dark energy is negligible and the energy is conserved. Using the energy conservation for the spherical region with a radius  $R$  and a mass  $M$  yields:

$$\dot{R}^2 = 2 \left[ E + \frac{GM}{R} \right] \quad (18)$$

the potential energy at every time is:

$$2 \frac{GM}{R} = (H_0 R)^2 \left[ \Omega_m (1 + \delta) a^{-3} + \Omega_\Lambda (a; b, w_0) \right], \quad (19)$$

using  $M = M_i$ , we get:

$$\left(\frac{R}{a}\right)^3 (1 + \delta) = \left(\frac{R_i}{a_i}\right)^3 (1 + \delta_i), \quad (20)$$

therefore by using equations (17), (19) and (20) we obtain for the size evolution of the spherical region  $R$  in the Eq. (18):

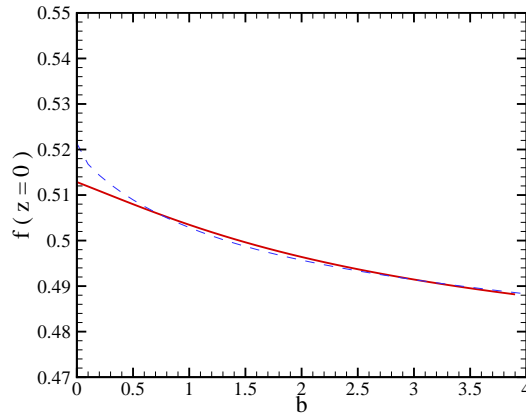


Fig. 6. The growth index  $f$  at the present time as a function of the bending parameter  $b$  for a flat universe with  $\Omega_m = 0.3$  and  $\Omega_\lambda = 0.7$ . The solid line is given by the numerical solution of Eq. (15) and dashed-line is given by fitting formula (Eq. (16)).

$$\frac{\dot{R}^2}{H_0^2} = \frac{\Omega_m(1 + \delta_i)}{a_i^3} \frac{R_i^3}{R} + \Omega_\lambda R^2 a^{-3[1+\bar{w}(a;b,w_0)]} - \Omega_m \delta_i \frac{R_i^2}{a_i^3} - (\Omega_{tot} - 1) \left(\frac{R_i}{a_i}\right)^2. \quad (21)$$

After the time  $t_i$  the scale factor  $a$  evolves according to the Friedmann equation and the spherical region changes its size with Eq. (21). For the numerical solution of this equation we replace  $\dot{R}$  by  $dR/da$ . Fig. 7 shows the evolution of  $R$  as a function of scale factor  $a$ . In agreement with the results obtained by the linear perturbation theory (Fig. 3), Section 2, we also see a suppression of the growth of overdense and underdense regions if we increase  $b$ . Although the effect on the dynamical growth of spherical underdense regions seems to be very small, its tendency is discovered by observational data. It has been shown for example in <sup>26,27</sup>, that large voids have a lower abundance in the cosmological  $N$ -body simulations than in the observations of the large scale in redshift surveys. The effect of a variable dark energy would slightly increase this discrepancy.

#### 4. Observational constraints

In this section we examine the constraints on the free parameters of the model from the observational data of the large scale structure (LSS) and SNIa. Observational constraints from the CMB and the amplitude of baryonic oscillations peak from the luminous red galaxies in Sloan Digital Survey Sky (SDSS) can be found in <sup>14</sup>.

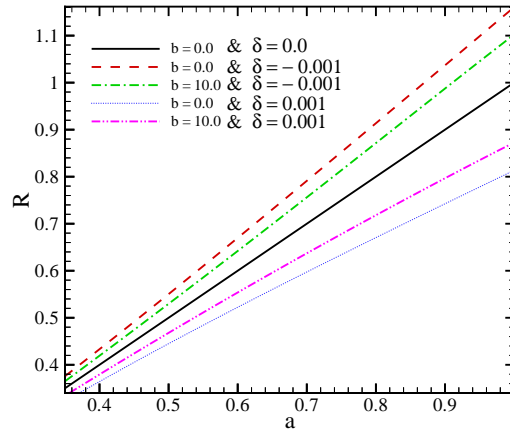


Fig. 7. Evolution of radius of a spherical overdense or underdense perturbation as a function of scale factor for different bending parameters. The initial conditions are  $z_i = 1100$  and  $\delta_i$  as denoted in the diagram.

#### 4.1. Constraints from Supernovae Type Ia

The SNIa experiments provide the most important indication for the existence of dark energy in the standard model of cosmology. Since 1995 two teams, the High-Z Supernovae Search, and the Supernovae Cosmology Project have discovered several SNIa candidates at high redshifts<sup>28,29</sup>. In<sup>4</sup> the discovery of 16 SNIa the Hubble Space Telescope were announced containing some of the most distant ( $z > 1.25$ ) SNIa known to date. Based on this data a uniform Gold sample of high and low redshift SNIa was constructed,<sup>4,30,31</sup>. In this subsection we compare the predictions of the dark energy model with the SNIa Gold sample. The observations of Supernovae measure essentially the apparent magnitude  $m$  including reddening, K correction etc, which is related to the (dimensionless) luminosity distance,  $D_L$ , of a an object at redshift  $z$ , for a spatially flat universe by:

$$m = \mathcal{M} + 5 \log D_L(z; b, w_0), \quad (22)$$

where for arbitrary spacial geometry

$$D_L(z; b, w_0) = \frac{H_0(1+z)}{\sqrt{|\Omega_K|}} \text{sinn} \left( \sqrt{|\Omega_K|} \int_0^z \frac{1}{H(\zeta; b, w_0)} d\zeta \right), \quad (23)$$

where  $\Omega_K = 1 - \Omega_m - \Omega_\Lambda$ , and "sinn" is "sinh" for  $k > 0$  (closed Universe) and "sin" for  $k < 0$  (open Universe)<sup>32</sup>. For  $k = 0$ , Eq. (23) reduces to  $H_0(1+z)$  times the integral. Also

$$\mathcal{M} = M + 5 \log_{10} \left( \frac{c/H_0}{1 \text{ Mpc}} \right) + 25, \quad (24)$$

where  $M$  is the absolute magnitude. The distance modulus,  $\mu$ , is defined as:

$$\mu \equiv m - M = 5 \log_{10} D_L(z; b, w_0) + 5 \log_{10} \left( \frac{c/H_0}{1 \text{ Mpc}} \right) + 25, \quad (25)$$

In order to compare the theoretical results with the observational data, we must compute the distance modulus, as given by Eq. (25). The first step in this sense is to compute the quality of the fitting through the least squared fitting quantity  $\chi^2$  defined by:

$$\chi^2 = \sum_i \frac{[\mu_{obs}(z_i) - \mu_{th}(z_i; \Omega_m, w_0, b, h)]^2}{\sigma_i^2}, \quad (26)$$

where  $\sigma_i$  is the observational uncertainty in the distance modulus. To constrain the parameters of model, we use the Likelihood statistical analysis. The method and its motivation are described in detail in ref.<sup>33</sup>. In the absence of prior constraint, the probability of the set of distance modulus  $\mu$  conditional on the values of a set of model parameters is given by a product of Gaussian functions:

$$p(\mu_{th}(z_i; \{l\})) = \prod_i \frac{1}{\sqrt{2\pi\sigma_i^2}} \exp \left[ -\frac{[\mu_{obs}(z_i) - \mu_{th}(z_i; \{l\})]^2}{2\sigma_i^2} \right], \quad (27)$$

where  $\{l\} = \{\Omega_m, w_0, b, h\}$ . This probability distribution must be normalized. Evidently, when, for a set of values of the parameters, the  $\chi^2$  is minimum the probability is maximum. We find the minimum value of  $\chi^2_{min}/N_{d.o.f} = 1.131$  corresponding to the best fit values for the model parameters  $h = 0.66$ ,  $w_0 = -1.90^{+0.75}_{-3.29}$ ,  $\Omega_m = 0.01^{+0.51}_{-0.01}$  and  $b = 6.00^{+7.35}_{-6.00}$  at  $1\sigma$  level of confidence. As a special case we fix the value of the state parameter to  $w_0 = -1.0$  and obtain the best fit values for the model parameters as:  $h = 0.65$ ,  $\Omega_m = 0.01^{+0.14}_{-0.01}$  and  $b = 2.08^{+0.40}_{-0.98}$  at  $1\sigma$  confidence level with  $\chi^2_{min}/N_{d.o.f} = 1.133$ . The values of cosmological parameters from fitting the dark energy model are different from those in the  $\Lambda$ CDM model, i.e. the value of  $h = 0.71^{+0.04}_{-0.03}$  and  $\Omega_m = 0.27^{+0.04}_{-0.04}$  are slightly smaller in the WMAP results for  $\Lambda$ CDM model<sup>34,35</sup>. If we use the Hubble parameter  $H_0 = 71.0 \pm 7.0$  from the HST-Key project as a prior parameter, the best fit values are:  $\Omega_m = 0.00^{+0.01}_{-0.00}$  and  $b = 0.79^{+0.13}_{-0.13}$  at  $1\sigma$  confidence level with  $\chi^2_{min}/N_{d.o.f} = 1.552$ . The values of model parameters with  $1\sigma$  and  $2\sigma$  confidence levels are summarized in Table 1 and 2. Figures 8, 9 and 10 show marginalized relative probability density functions for cosmological parameters.

#### 4.2. Combined Constraints from Structure formation and SNIa

The above analysis shows that the SNIa data alone does not sufficiently constrain the variable dark energy model. Furthermore the fit of SNIa data is sensitive to the parameter  $H_0$ . Hence, it is very important to find other observational quantities independent of  $H_0$  as a complement to the SNIa data. In the pervious sections we studied the effect of varying dark energy model on the evolution of large scale structures. Here we use the results from the 2dFGRS data and combine this with the SNIa data to put more rigorous constraint on the parameters of variable dark energy model.

The 2dFGRS contains the observation of the position and the redshift of about 220,000 galaxies. On this basis the 2dFGRS team has determined a growth index  $f$ , which is the relevant parameter for the comparison with the predictions of the dark energy model<sup>36</sup>. From measuring the two-point correlation function, they report the redshift distortion parameter  $\beta = f/\tilde{b} = 0.49 \pm 0.09$  at  $z = 0.15$ , where  $\tilde{b}$  is the bias parameter describing the difference in the distribution of galaxies and mass. Verde et al. (2003) used the bispectrum of 2dFGRS galaxies<sup>37,38</sup> and obtained  $\tilde{b}_{verde} = 1.04 \pm 0.11$ , from which, we obtain  $f(z = 0.15) = 0.51 \pm 0.10$ .

We perform a combined analysis of the SNIa and Large Scale Structure (LSS) to constrain of variable dark energy model through  $\chi^2$  fitting:

$$\chi^2 = \chi^2_{\text{SNIa}} + \chi^2_{\text{LSS}}, \quad (28)$$

where  $\chi^2_{\text{SNIa}}$  is given by Eq. (26) for SNIa data and  $\chi^2_{\text{LSS}}$  is the contribution of LSS data using Eq. (15). The best fit values for the model parameters are:  $h = 0.66$ ,  $\Omega_m = 0.21^{+0.07}_{-0.06}$ ,  $b = 4.05^{+7.05}_{-2.25}$  and  $w_0 = -2.05^{+0.65}_{-2.05}$  at  $1\sigma$  confidence level with the corresponding  $\chi^2_{min}/N_{d.o.f} = 1.131$ . The values of model parameters for  $1\sigma$  and  $2\sigma$

confidence levels using SNIa+LSS observations are given in Table 1. Fig. 8 shows the marginalized relative likelihood functions (upper panel) and joint confidence contours (lower panel) of the model parameters.

Further, we restrict the analysis to a subset of the parameter space and fix the present state parameter at  $w_0 = -1.0$ . Again using the combined LSS and SNIa data, the best fit values for the model parameters are  $h = 0.64$ ,  $\Omega_m = 0.20^{+0.07}_{-0.05}$  and  $b = 0.80^{+0.45}_{-0.60}$  with  $\chi^2_{min}/N_{d.o.f} = 1.142$  at  $1\sigma$  confidence level. The values of the model parameters for  $1\sigma$  and  $2\sigma$  confidence levels are reported in Table 2. Fig. 9 shows the marginalized relative likelihood functions of matter density and the bending parameter. If we use  $H_0 = 71.0 \pm 7.0$  from the HST-Key project as a prior with  $1\sigma$  measurement, we obtain the best fit values of the model parameters at  $\Omega_m = 0.10^{+0.04}_{-0.03}$ ,  $b = 0.20^{+0.25}_{-0.20}$  at  $1\sigma$  confidence level with  $\chi^2_{min}/N_{d.o.f} = 1.618$ . The marginalized relative likelihood functions of the matter density and the bending parameter are shown in Fig. 10.

Finally we determine the predicted age of universe considering the parameters of the model according to:

$$t_0(b, w_0) = \int_0^{t_0} dt = \int_0^\infty \frac{dz}{(1+z)H(z; b, w_0)}, \quad (29)$$

and compare it with the age of old objects in the universe as a consistency test. In Table 1 we show that the age of universe from SNIa and the combined SNIa+LSS analysis are  $13.45^{+3.39}_{-2.34}$  Gyr and  $13.54^{+2.34}_{-3.75}$  Gyr, respectively, which is in the range of the age of old stars  $13^{+4}_{-2}$  Gyr<sup>39</sup>.

Furthermore we use the observed age of three Old High Redshift Galaxies (OHRG) for comparison with the dark energy model, namely the LBDS 53W091, a 3.5-Gyr-old radio galaxy at  $z = 1.55$ <sup>40</sup>, the LBDS 53W069, a 4.0-Gyr-old radio galaxy at  $z = 1.43$ <sup>41</sup> and a quasar, APM 08279 + 5255 at  $z = 3.91$  with an age of  $t = 2.1^{+0.9}_{-0.1}$  Gyr<sup>42</sup>. The latter one has once led to the "age crisis" in the  $\Lambda$ CDM model<sup>43</sup>. To quantify the age consistency test we introduce the expression  $\tau$  as:

$$\tau = \frac{t(z; b, w_0)}{t_{obs}}, \quad (30)$$

where  $t(z; b, w_0)$  is the predicted age of universe from Eq. (29) and  $t_{obs}$  is an estimation for the age of the old object. In order to have a compatible predicted age of the universe, it is necessary to have  $\tau \geq 1$ . Table 3 shows the values of  $\tau$  for three mentioned OHRG. If we fix the parameters within the  $1\sigma$  confidence level of the above combined observational constraints of SNIa and LSS, the predicted age of the universe is larger than the age of LBDS 53W069 and LBDS 53W091, while APM 08279 + 5255 at  $z = 3.91$  is older. Only in the case that we fix  $w_0 = -1$  and  $H_0 = 71.0 \pm 7.0$  from HST-Key project, we obtain  $\tau > 1$ .

## 5. Conclusions

In this paper we have considered a simple model for variable dark energy and examined its influence on the cosmological structure formation. First we have used

the Newtonian linear perturbation theory to see the possible effects of a quintessence model, which is parameterized according to a prescription given by Wetterich (2004). The crucial parameter of this scheme is the bending parameter  $b$ , which changes the behavior of dark energy toward a more dust-like behavior. Considering a flat, an open and a closed universe and an almost arbitrary initial value of the density contrast  $\delta$ , we find that by increasing the bending parameter, the growth of the  $\delta$  is decreased in comparison to the conventional  $\Lambda$ CDM model. In agreement with the results of our nonlinear spherical calculations, we find that increasing the bending parameter reduces the rate of growth of structure. This suppression in the growth of structure occurs in all open, flat and closed models for sufficiently large values of  $b$ .

This effect can be explained by the fact that the dominance of the dark energy term occurs earlier with respect to  $\Lambda$ CDM, the larger the parameter  $b$  is. Because

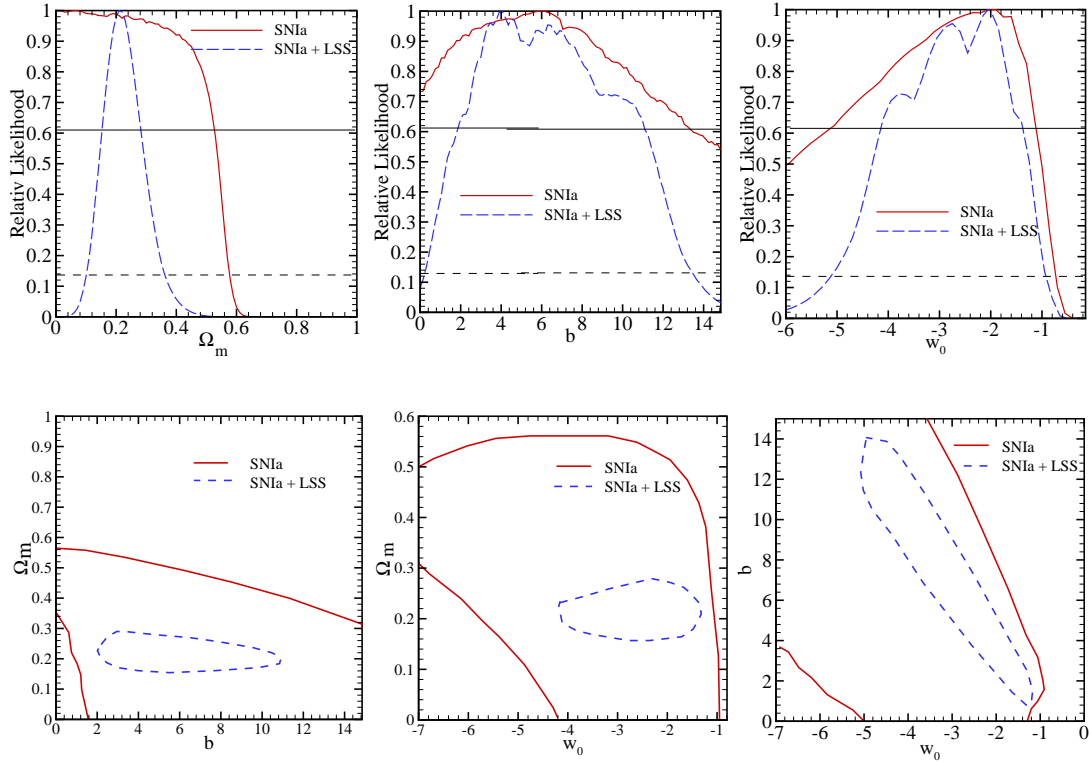


Fig. 8. The upper panel shows marginalized likelihood functions of cosmological parameters. The solid line was obtained by marginalizing over all nuisance parameters, using SN Ia and dashed-line corresponds to SN Ia+LSS. The intersections with the horizontal solid and dashed lines give the bounds for 68.3% and 95.4% confidence respectively. The lower panel shows joint confidence contours with  $1\sigma$  confidence level.

of the earlier domination of dark energy, the rate of the structure formation process is decreased. This finding is also supported by the second part of our calculations, where we numerically solve the equation of the collapse of a spherically symmetric density perturbation. We also give the fitting formula for the growth index,  $f$ , at the present time as a function of model parameters. the leading term of this formula

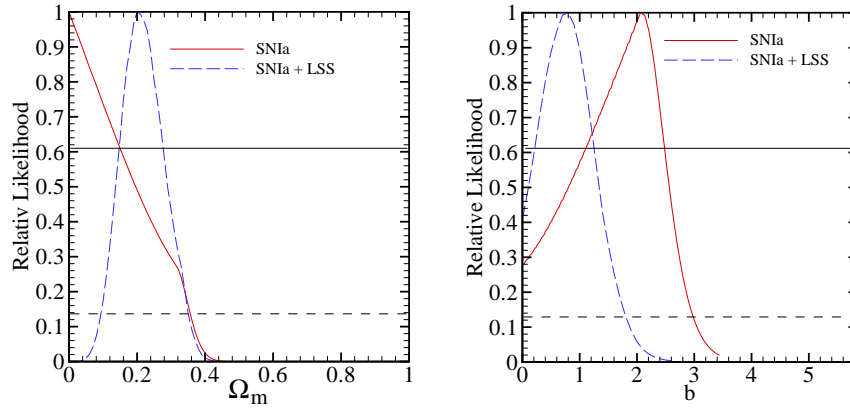


Fig. 9. The marginalized likelihood functions of cosmological parameters. The solid line was obtained by marginalizing over all nuisance parameters, using SNIa and dashed-line corresponds to SNIa+LSS. The intersections with the horizontal solid and dashed lines give the bounds for 68.3% and 95.4% confidence respectively. Here we assume  $w_0 = -1.0$ .

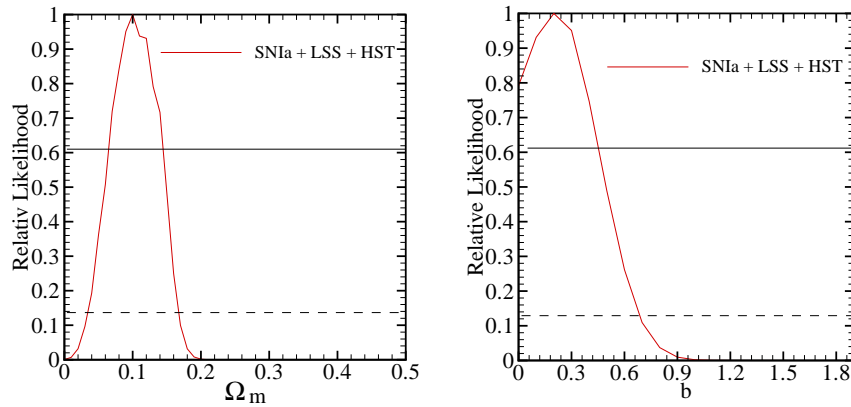


Fig. 10. Marginalized likelihood functions of cosmological parameters. The solid line was obtained by marginalizing over all nuisance parameters, using SNIa+LSS+HST. HST prior is  $H_0 = 71.0 \pm 7.0$ . The intersections with the horizontal solid and dashed lines give the bounds for 68.3% and 95.4% confidence respectively. Here we assume  $w_0 = -1.0$ .

is  $\Omega_m^\alpha$  which is in agreement with  $\Lambda$ CDM models<sup>44,45,46</sup>.

In order to constrain the model parameters, we used the Gold sample SNIa data. The SNIa analysis resulted in a large degeneracy between the model parameters. For improving this, we perform a joint analysis of the SNIa and LSS data. This joint analysis of SNIa+LSS produces more reasonable results:  $h = 0.66$ ,  $\Omega_m = 0.21_{-0.06}^{+0.07}$ ,  $w_0 = -2.05_{-2.05}^{+0.65}$  and  $b = 4.05_{-2.25}^{+7.05}$ , at  $1\sigma$  confidence level with  $\chi_{min}^2/N_{d.o.f} = 1.131$ . The age of universe from the best fit values of model parameters by using SNIa+LSS is  $13.54_{-3.74}^{+2.34}$  Gyr, which is compatible with the age of old stars. We also chose three high redshift radio galaxies namely the LBDS 53W091, a 3.5-Gyr-old radio galaxy at  $z = 1.55$ , the LBDS 53W069, a 4.0-Gyr-old radio galaxy at  $z = 1.43$  and a quasar, APM 08279 + 5255 at  $z = 3.91$  with an age of  $t = 2.1_{-0.1}^{+0.9}$  Gyr. The age of the two first objects is consistent with the age of universe using the best fit values of the model parameters, while the later one is older than the universe. The age of quasar APM 08279 + 5255, was also the reason of the "age crisis" for the  $\Lambda$ CDM model and it is compatible with the dark energy model only if we fix  $w_0 = -1.0$  and assume the Hubble parameter at the value given by HST-Key project as a prior in our calculations.

### Acknowledgments

The authors thank Niyayesh Afshordi and Volker Müller for their useful comments.

### References

1. A.G. Riess et al., ApJ, **116**, 1009 (1998).
2. A.G. Riess, PASP, **112**, 1284 (2000).
3. S. Perlmutter et al., ApJ, **517**, 565 (1999).
4. A. G. Riess et al., ApJ, **607**, 665 (2004).
5. Ya. B. Zeldovich, Pis'ma Zh. Eksp. Teor. Fiz., **6**, 883 (1967).
6. S. Weinberg, Rev. Mod. Phys., **61**, 1 (1989).
7. S.M. Carroll, "The Cosmological Constant", Living Rev. Relativity, **4**, 1 (2001).
8. R. Caldwell, R. Dave, P. Steinhardt, PRL D **59**, 123504 (1999).
9. C. Wetterich, Nucl. Phys. B, **302**, 668 (1988).
10. B. Ratra and P. J. E. Peebles, Phys. Rev. D **37**, 3406 (1988).
11. V. Sahni, In S. Rahvar, N. Sadooghi, F. Shojai, eds, Proc. of XI Regional Conf. on Math. Phys., The Mysterious nature of dark energy, World Scientific Press (2005).
12. C. Wetterich, Physics Lett. B, **594**, 17 (2004).
13. M. Doran, K. Karwan and C. Wetterich, JCAP, **007** 0511 (2005).
14. M.S. Movahed and S. Rahvar, Phys. Rev. D **73**, 083518 (2006).
15. S. W. Allen, R. W. Schmidt, H. Ebeling, A. C. Fabian and L. Van Speybroeck, MNRAS, **353**, 457 (2004).
16. R. A. Daly and S. G. Djorgovski, ApJ, **597**, 9 (2003).
17. R. A. Daly and S. G. Djorgovski, ApJ, **612**, 652 (2004).
18. D. N. Spergel et al., [WMAP Collaboration], ApJ Suppl. **148**, 175 (2003).
19. T. Padmanabhan, Structure Formation in the Universe. Cambridge Univ. Press (1993).
20. R. H. Brandenberger in N. Breton, J. L. Cervantes-Cota and M. Salgado eds, Lecture Notes in Physics, The early universe and observational cosmology, 646, p.127 (2004).



21. P. J. E. Peebles, *The Large Scale Structure of the Universe*, Princeton University Press, Princeton, NJ (1980).
22. R. Mansouri and S. Rahvar, *IJMPD*, **11**, 312 (2002).
23. O. Lahav, P. B. Lilje, J. R. Primack and M. J. Rees, *MNRAS*, **251**, 128 (1991).
24. S. Gottlöber E. Lokas, A. Klypin and Y. Hoffman, *MNRAS*, **344**, 715 (2003).
25. Y. Friedmann and T. Piran, arXiv:astro-ph/0009320.
26. S. Arbabi-Bidgoli and V. Müller, *MNRAS*, **332**, 205 (2002).
27. Müller, V., Arbabi-Bidgoli, S., Einasto, J., & Tucker, D. 2000, *MNRAS*, **318**, 280
28. B. P. Schmidt et al., *ApJ* **507**, 46 (1998).
29. S. Perlmutter, M.S. Turner and M. White, *Phys. Rev. Lett.* **83**, 670 (1999).
30. J. L. Tonry et al., *ApJ* **594**, 1 (2003).
31. B. J. Barris et al., *ApJ* **602**, 571 (2004).
32. S.M. Carroll, W.H. Press and E.L. Turner, *ARA&A*, **30**, 499 (1992).
33. Jr. R.Colistete , J.C. Fabris, S. V. B. Goncalves and P. E. de Souza , *Int. J. Mod. Phys. D13*, 669 (2004).
34. D. N. Spergel et al., *ApJ* **148**, 175 (2003).
35. S. Eidelman et al., (Particle Data Group), *Phys. Lett. B* **592**, 92 (2004).
36. D. J. Eisenstein et al., astro-ph/0501171.
37. L. Verde, M. Kamionkowski, J.J. Mohr, A. J. Benson, *MNRAS*, **321**, L7 (2001).
38. O. Lahav, S. L. Bridle, W. J. Percival, & the 2dFGRS Team, *MNRAS*, **333**, 961 (2002).
39. E. Carretta et al., *ApJ*, **533**, 215 (2000).
40. J. Dunlop et. al., *Nature (London)* **381**, 581 (1996).
41. J. Dunlop, in *The Most Distant Radio Galaxies*, edited by H. J. A. Rottgering, P. Best, and M. D. Lehnert (Kluwer, Dordrecht, 1999), p. 71.
42. G. Hasinger, N. Scharrel and S. Komossa, *ApJ Lett.* **573**, L77 (2002).
43. D. Jain, A. Dev, astro-ph/0509212 (accepted in *Phys. Lett. B*)
44. V. Silveria and I. Waga, *phys. Rev. D*, **50**, 4890 (1994).
45. L. Wang and P.J. Steinhardt, *ApJ*, **508**, 483 (1998).
46. E.L. Lokas, P. Bode and Y. Hoffman, *MNRAS*, **349**, 595 (2004).

Table 1. Estimated variable dark energy model parameters (mean, 68.3%, 95.4% C.L.), including the present matter density, the bending parameter, the state parameter and the age of Universe.

Observation	$\Omega_m$	$b$	$w_0$	age (Gyr)
SNIa	$0.01^{+0.51}_{-0.01}$	$6.00^{+7.35}_{-6.00}$	$-1.90^{+0.75}_{-3.29}$	$13.45^{+3.39}_{-13.45}$
	$0.01^{+0.56}_{-0.01}$	$6.00^{+17.42}_{-6.00}$	$-1.90^{+1.10}_{-7.23}$	
SNIa+LSS	$0.21^{+0.07}_{-0.06}$	$4.05^{+7.05}_{-2.25}$	$-2.05^{+0.65}_{-2.05}$	$13.54^{+2.34}_{-3.74}$
	$0.21^{+0.17}_{-0.11}$	$4.05^{+9.20}_{-3.75}$	$-2.05^{+1.10}_{-3.10}$	

Table 2. Estimated variable dark energy model parameters (mean, 68.3%, 95.4% C.L.) for the fixed value of the state parameter  $w_0 = -1$ , including the present matter density, the bending parameter and the age of Universe assuming  $w_0 = -1.0$ . The HST prior is set at  $0.71 \pm 0.07$ .

Observation	$\Omega_m$	$b$	age (Gyr)
SNIa	$0.01^{+0.15}_{-0.01}$	$2.08^{+0.40}_{-0.98}$	$14.23^{+1.27}_{-2.20}$
	$0.01^{+0.35}_{-0.01}$	$2.08^{+0.89}_{-2.08}$	
SNIa+HST	$0.00^{+0.01}_{-0.00}$	$0.79^{+0.13}_{-0.13}$	$16.66^{+0.64}_{-1.09}$
	$0.00^{+0.06}_{-0.00}$	$0.79^{+0.28}_{-0.36}$	
SNIa+LSS +HST	$0.10^{+0.04}_{-0.03}$	$0.20^{+0.25}_{-0.20}$	$16.72^{+1.52}_{-1.43}$
	$0.10^{+0.06}_{-0.07}$	$0.20^{+0.45}_{-0.20}$	
SNIa+LSS	$0.20^{+0.07}_{-0.05}$	$0.80^{+0.46}_{-0.60}$	$14.55^{+1.04}_{-1.44}$
	$0.20^{+0.15}_{-0.10}$	$0.80^{+0.90}_{-0.80}$	

Table 3. Estimated relative age  $\tau$  of three high redshift objects using the best fit values of model parameters with  $1\sigma$  confidence level.

Observation	LBDS 53W069 $z = 1.43$	LBDS 53W091 $z = 1.55$	APM 08279 + 5255 $z = 3.91$
SNIa+ $w_0 = -1$	$1.13^{+0.31}_{-0.55}$	$1.21^{+0.36}_{-0.63}$	$0.78^{+0.69}_{-0.78}$
SNIa+HST+ $w_0 = -1$	$1.67^{+0.16}_{-0.27}$	$1.81^{+0.18}_{-0.31}$	$1.26^{+1.10}_{-0.52}$
SNIa+LSS+ $w_0 = -1$	$1.19^{+0.26}_{-0.36}$	$1.27^{+0.30}_{-0.41}$	$0.84^{+0.61}_{-0.68}$
SNIa+LSS+HST+ $w_0 = -1$	$1.63^{+0.38}_{-0.35}$	$1.75^{+0.43}_{-0.41}$	$1.19^{+0.88}_{-0.68}$
SNIa	$1.00^{+0.84}_{-1.00}$	$1.05^{+0.96}_{-1.05}$	$0.65^{+1.63}_{-0.65}$
SNIa+LSS	$1.00^{+0.58}_{-0.93}$	$1.06^{+0.67}_{-1.06}$	$0.67^{+1.15}_{-0.67}$